

Highlights

A general hierarchical control system to model ACC systems: an empirical study

Tiancheng Ruan,Hao Wang,Linjie Zhou,Rui Jiang,Xinjian Xie

- A general hierarchical control system is developed to model the ACC system.
- A phenomenon of multiple time delays is raised and verified by field data.
- A new general fitted model with higher goodness of fit is proposed.
- Insights into optimization strategy on string stability.

A general hierarchical control system to model ACC systems: an empirical study

Tiancheng Ruan^{a,b,c}, Hao Wang^{a,b,c,*}, Linjie Zhou^{a,b,c}, Rui Jiang^{d,*} and Xinjian Xie^e

^aJiangsu Key Laboratory of Urban ITS, Southeast University, 2 Si Pai Lou, Nanjing, 210096, P.R. China

^bJiangsu Province Collaborative Innovation Center of Modern Urban Traffic Technologies, 2 Si Pai Lou, Nanjing, 210096, P.R. China

^cSchool of Transportation, Southeast University, 2 Si Pai Lou, Nanjing, 210096, P.R. China

^dKey Laboratory of Transport Industry of Big Data Application Technologies for Comprehensive Transport, Ministry of Transport, Beijing Jiaotong University, Beijing, 100044, P.R. China

^eGuangzhou Baiyun Airport Customs District, Renhe town, Guangzhou, 510470, P.R. China

ARTICLE INFO

Keywords:

Adaptive cruise control
String stability
field experiments
hierarchical control system

ABSTRACT

Urged by a close future perspective of a traffic flow made of a mix of human-driven vehicles and automated vehicles (AVs), research has recently focused on studying the traffic flow characteristics of Adaptive Cruise Controls (ACCs), the most typical AV. However, in most works, the ACC system is studied under a simplifying and unrealistic assumption, or the ACC system modeled is inaccurate. This paper proposes a general hierarchical control system to model ACC systems with several assumptions based on the deficiencies above. Moreover, a field experiment was conducted, and the corresponding experimental data was used to verify the proposed hierarchical control system and assumptions. In addition, string stability is explored along with sensitivity analyses of control parameters based on an example under the constant time gap policy. The results show that different upper level controller parameters have different delays, where the delay of the speed is negligible; the introduction of actuator delay and lag in the lower level controller can significantly improve the model goodness of fit. Furthermore, optimizing the delay and lag in the lower level controller can significantly enhance the string stability of ACCs than optimizing the control parameters.

1. Introduction

Since the invention of the automobile over a century ago, automotive engineers have been working to provide safer and more comfortable services. However, traffic congestion, accidents, and pollutant emissions have become increasingly prominent in past decades (Schrank et al., 2012; Jin and Orosz, 2016). Traditional traffic engineering improves road capacity and level of service through external measures like traffic management, traffic control, and so forth. However, these methods are gradually facing bottlenecks. By studying the dynamic and static characteristics of traffic flow, it can be found that the uncertainty in road traffic is caused by the extensive heterogeneity of humans (Zhong et al., 2020; Ye and Yamamoto, 2018; van Arem et al., 2016; Yu et al., 2021). This leads to poor traffic flow stability, limited traffic capacity, and frequent traffic accidents.

For the above traffic problems, Autonomous Vehicle (AV) stands out as a promising enabler and has gained significant popularity in academia and the automotive industry in recent years. Despite its relatively short history, plentiful research has demonstrated its advantages regarding safety, emissions, and capacity over human drivers (Wang et al., 2019; Sarker et al., 2019; Dey et al., 2015). As the most typical example of AV, Adaptive Cruise Control (ACC) systems tracks the predecessor based on on-board sensory devices to maintain a constant gap/time gap. They are becoming increasingly available as standard equipment in modern commercial vehicles with the market penetration rate (MPR) increasing (Wilson and Ward, 2011). Parallel to ACC systems, another paradigm is Cooperative Adaptive Cruise Control (CACC) systems using Vehicle-to-Infrastructure (V2I) / Vehicle-to-Vehicle (V2V) communication to improve safety and capacity further.

Unfortunately, it will take a long time for CACC MPR to grow due to the immaturity of CACC technology, as the CACC MPR is projected to be only 24.8% in 2045, according to the latest research (Bansal and Kockelman, 2017).

*Corresponding author

 ruantiancheng@seu.edu.cn (T. Ruan); haowang@seu.edu.cn (H. Wang); 220193107@seu.edu.cn (L. Zhou); jiangrui@bjtu.edu.cn (R. Jiang); gzxxj_124688@163.com (X. Xie)

ORCID(s):

Moreover, since a small amount of CACCs cannot guarantee that communication functions properly, most CACCs will degrade into ACCs (Wang et al., 2018; Ruan et al., 2021; Zhou et al., 2021). Therefore, research on ACCs is still necessary because ACCs will remain mainstream for a long time, although CACCs can perform better.

Although extensive research has been conducted on ACC systems, it is still unclear what impacts ACC vehicles will make on traffic flow. Several theoretical studies explore the effects of ACCs on capacity and fundamental diagrams (Shang and Stern, 2021; Li et al., 2022; Ciuffo et al., 2021), while others analyze the stability of ACCs (Flores and Milanés, 2018; Lee et al., 2021; Zhou et al., 2017). However, existing studies have inadequately modeled ACC systems, and a large number of studies have been conducted on this (Gunter et al., 2019; Shang et al., 2022; Milanés and Shladover, 2014). Albeit corresponding research about ACC systems has been conducted for many years, the theoretical analysis of most of the research still focuses only on the upper level controller. It ignores the role played by the lower level controller, which makes the results of the theoretical analysis inconsistent with the field data. On the other hand, an unreasonable assumption is adopted in existing studies that all upper level controller parameters do not have a time delay or have the same time delay (Ngoduy, 2013a; Zhou and Ahn, 2019).

To fill the gap, this paper models the ACC system precisely and verifies it by field data. The main contributions of this paper are:

1. A general hierarchical control system consisting of an upper level controller and a lower level controller is developed to model the ACC system.
2. A phenomenon is raised that different parameters in the general upper level controller have different delays based on the characteristics of the on-board sensory devices and verified by field data.
3. Based on the mechanism of the lower level controller, a new general fitted model is proposed and verified by comparison that the new model has higher goodness of fit.
4. An ACC example under CTG control strategies is chosen to explore the stable regions under different control parameters for giving new insights into the design of control strategies.
5. Sensitivity analysis of different device parameters is conducted to guide control strategy optimization.

The remainder of the paper is outlined as follows: Section 2 introduces the hierarchical control ACC system consisting of an upper level controller and a lower level controller. Section 3 presents the field experiments and verifies the rationality of the assumptions in the general hierarchical control system by field data. Corresponding string stability is analyzed based on an ACC example under CTG strategy in Section 4. We summarize the study in Section 5.

2. Model formulation

In this section, we systematically introduce the mechanism of ACC systems. Furthermore, we propose a general hierarchical control system to model ACC systems based on this. It is worth noting that the general system in this article can degrade to the system adopted in the existing literature by ignoring the assumptions of the mechanism.

2.1. General hierarchical control system

The primary objective of the ACC control system is to track the predecessor based on on-board sensory devices to maintain a constant gap/time gap. This objective is simplified to execute steady-state and transient longitudinal maneuvers in single-lane traffic flow. Considering ACC system structure, it is designed as a hierarchical control system with an upper level controller and a lower level controller, as shown in Fig. 1. The upper level controller determines the desired longitudinal acceleration for each vehicle. The lower level controller determines the throttle and/or brake commands required to track the desired acceleration. Vehicle dynamic models, engine maps, and nonlinear control synthesis techniques (Choi and Devlin, 1995; Choi and Hedrick, 1995; Hedrick et al., 1991, 1993) are used by the lower level controller in calculating the real-time brake and throttle inputs required to track the desired acceleration.

This paper explores the specific model forms of upper and lower models based on the experiment results. Noting, $x_i(t)$, $v_i(t) = \dot{x}_i(t)$, $a_i(t) = \ddot{x}_i(t)$, and $\dot{a}_i(t) = \dddot{x}_i(t) \in \mathbb{R}$ are used to denote the longitudinal position, speed, acceleration, and jerk of vehicle i at time t , respectively.

2.2. General upper controller

The objective of the upper controller is to determine desired acceleration based on the specific parameters obtained from the surrounding environment by sensors. Different from the integrated process of human perception, the various parameters required by the upper controller are acquired based on different sensors and naturally have different sensor

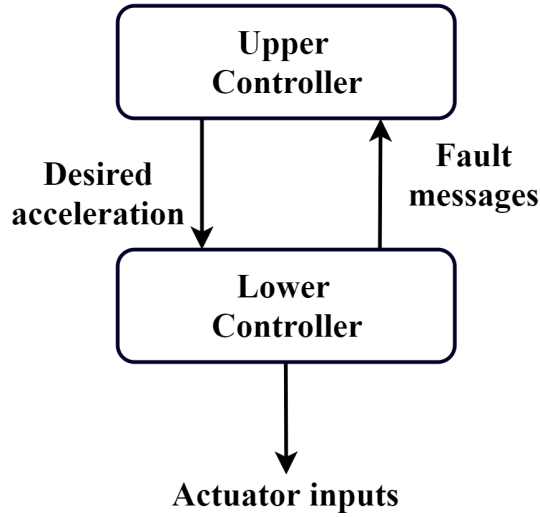


Figure 1: Structure of ACC control system.

delays according to the characteristics of the sensor. There have been several studies that have proposed this, but there is still a lack of sufficient experiments to prove it (Ngoduy, 2013b; Yao et al., 2021).

Sensor delay is caused by the process of sensing and filtering due to the discrete sampling of on-board measurements, the radar or lidar filtering, and the bandwidth of low pass filters used for other sensors such as wheel speed sensors. Due to differences in the sensor devices equipped, the sensor delay is uncertain (Loke, 2019).

For ACC systems, the parameters required by the upper-level controller mainly include the speed, the gap between the subject vehicle and its predecessor, and the relative speed between the subject vehicle and its predecessor. The principle of the sensor acquiring the first two parameters is similar to most existing vehicle configurations. However, there is disagreement about how the relative speed between the subject vehicle and its predecessor is measured. Based on the principle of the sensors, the method is divided into the case with the relative speed and with the lead speed. The former obtains the relative speed by Doppler measurement. The latter is to first return to the detection frame of the obstacle through laser detection and afterward select the tracking point based on the detection box. Then calculate the speed according to the position of the tracking point, which is carried out under the absolute coordinate system. After that, subtract from the current speed to obtain the corresponding relative speed. The general model forms under the two different measurement methods as follows.

2.2.1. The case with the relative speed

For the case of using Doppler measurement, since it is possible to get the relative speed with the predecessor directly through the sensor, the general upper controller is shown in Equation(1):

$$u_i = f(s_i(t - \eta_s), v_i(t - \eta_v), \Delta v_i(t - \eta_{dv})) \quad (1)$$

where u_i denotes the control input of the lower level controller; $f(\bullet)$ is the explicit equation corresponding to the control policy; $s_i = x_{i-1} - x_i - l_g - s_0$ stands for the gap from vehicle i to its predecessor $i - 1$; l_g is the vehicle length; s_0 represents the standstill gap; $\Delta v_i = v_{i-1} - v_i$ denotes the relative speed of vehicle i to its predecessor $i - 1$; η_s , η_v , and η_{dv} represent the sensor delays of gap, speed, and relative speed, respectively.

2.2.2. The case with the lead speed

For the case where the relative speed is obtained indirectly by measuring the lead speed and the speed of the subject vehicle, the general upper controller is shown in Equation(2):

$$u_i = f(s_i(t - \eta_s), v_i(t - \eta_v), v_{i-1}(t - \eta_{fv})) \quad (2)$$

where η_{fv} denotes the sensor delay of lead speed, and the definition of other parameters is the same as Equation(1).



Figure 2: Field experiments scene. (a) Vertical view of the experimental field; (b) Snapshots of the experiment.

It is worth mentioning that the delays of different parameters are set differently based on the assumption that different sensors acquire different parameters.

The caveat is that the time delays of different parameters in Equation(1) and Equation(2) are set differently based on the assumption that different parameters are obtained by different sensors, which is reasonable and general.

2.3. General lower level controller

In the lower level controller, the throttle and brake actuator inputs are determined so as to track the desired acceleration determined by the upper controller.

However, converting the desired acceleration into the actual acceleration is not clear. Existing researches generally assume that there is an engine actuator lag in this process, which implies that the commanded acceleration u_i cannot be realized instantaneously but only after a retarded time τ_i (Ploeg et al., 2011). The actuator lag lies in the lower level of the vehicle control system when executing the desired acceleration command from the upper ACC controller due to the time delay in the generation of traction/brake wheel torques in the power-train or brake actuator. Nevertheless, most of the existing research linearize vehicle dynamic as follows and regard actuator lag functions as a low pass filter (Wang, 2018; Naus et al., 2010):

$$G_i(s) = \frac{k_G}{\tau_i s + 1} \quad (3)$$

where $G_i(s)$ represents the transfer function of the lower level controller; k_G being the model gain, which, ideally, is equal to 1; τ_i denotes the engine actuator lag.

But, the aforementioned fitted expression we consider unreasonable because the actuator lag cannot be represented by the first-order inertial linker alone. Equation(3) only expresses the process of the power system receiving the control command u_i and realizing it to reach the actual acceleration \ddot{x}_i . The process by which the system receives control feedback, and calculates and delivers control commands to the power system is ignored. The control calculation of the latter is relatively simple, and the delivery of control commands is only carried out inside the vehicle system. However, it still needs to be clearly defined for a more accurate model modeling. The corresponding general model introduces actuator and internal communication delay as follows:

$$G_i(s) = \frac{k_G}{\tau_i s + 1} e^{-\phi_i s} \quad (4)$$

where ϕ_i denotes the actuator and internal communication delay, and the definition of other parameters is the same as Equation(3).

It is worth mentioning that Equation(4) can be degraded to Equation(3) by omitting ϕ_i . As for the effect of introducing ϕ_i on model accuracy, Section 3 compares fitted results based on experimental data. Moreover, Equation(3) and Equation(4) are linearized models from the nonlinear dynamic model. The linearization process is described in detail in Section 4.1.

3. Field experiments

3.1. Field experiments scene

Experiment preparation: The experiment was performed on Oct. 12, 2021, on an about 1.5-kilometer straight track in the test field affiliated with the Research Institute of Highway, Ministry of Transport, China. Six cycabs were used

Table 1

Parameters were chosen for different experiment round.

Experiment index	$K_v(s^{-2})$	$K_g(s^{-1})$	$T_g(s)$	$LeadV(m/s)$	Index of the deployed vehicle
1	0	0.3	3.2	20	1, 2, 3
2	0	0.3	3.2	20	1, 2, 3
3	0	0.3	2.5	20	1, 2, 3, 4, 5, 6
4	0	0.3	2.0	30	1, 2, 3, 4, 5
5	0.2	0.3	2.0	20	1, 2, 3, 4, 5, 6
6	0.2	0.3	2.0	20	1, 2, 3, 4, 5, 6
7	0.2	0.3	1.8	20	1, 2, 3, 4, 5, 6
8	0.2	0.3	1.8	20	1, 2, 3, 4, 5, 6
9	0.2	0.3	1.6	20	1, 2, 3, 4, 5, 6
10	0.2	0.3	1.6	20	1, 2, 3, 4, 5, 6
11	0.3	0.3	1.6	20	1, 2, 3, 4, 5, 6
12	0.3	0.3	1.6	30	1, 2, 3, 4, 5, 6
13	0.3	0.3	1.5	20	1, 2, 3, 4, 5, 6
14	0.3	0.3	1.5	30	1, 2, 3, 4, 5, 6
15	0.35	0.3	1.4	20	1, 2, 3, 4, 5, 6
16	0.35	0.3	1.4	30	1, 2, 3, 4, 5, 6

for experiments which were autonomous driving vehicles reconfigured from one CHANGAN AUTO CS55 PLUS, four CHANGAN AUTO CS55 E-Rocks, and one BAIC MOTOR ARCFOX α T for model years 2020, respectively. See Appendix 5 for the detailed information of experimental vehicles. The algorithm and parameter values of upper level controller of the cycabs can be set by the users. The scheme of LiDAR+ millimeter-wave + Ultrasonic radar + GPS inertial navigation was adopted as the navigation system, and the distance measurement accuracy is 0.01m. The decision frequency was 20 Hz which equals a 50ms decision interval. The measurement errors of the GPS devices were within ± 1 m for location and within ± 1 km/h for velocity. Fig. 2 indicates the scene of the field experiment where the while sport-utility vehicle with the lidar on its top is the employed AV and traffic lights do not function.

Experiment scheme: The experiment was carried out for 16 rounds. In each round, initially, the vehicles are stopped bumper-to-bumper. When an experimental run started, the leading vehicle accelerated to the given cruise speed and traveled at that speed until the end of the experimental run. Once the last vehicle stopped, the platoon made a U-turn and prepared for the next run. All vehicles moved straight ahead in the experiments and did not change lanes. The specific control parameters of the ACC system in different experiment round are shown in Table 1.

3.2. Upper controller

3.2.1. Data processing methods

Determination time delay: For the upper controller, what we need to determine is the sensor delays for different parameters based on experimental data. Since the measured and actual sequences in the raw data are two sets of error-prone and misaligned time sequences, we applied the Shape-Based Distance (SBD) algorithm based on the cross-correlation measure to determine the corresponding sensor delay (Paparrizos and Gravano, 2015). Cross-correlation is a statistical measure with which we can determine the similarity of two sequences $Z = (z_1, \dots, z_m)$ and $Y = (y_1, \dots, y_m)$, even if they are not properly aligned. To achieve shift-invariance, cross-correlation keeps Y static and slides X over Y to compute their inner product for each shift s of X . We denote a shift of a sequence as follows:

$$Z_{(s)} = \begin{cases} (0, \dots, 0, \underbrace{z_1, z_2, \dots, z_{m-s}}, \dots), & s \geq 0 \\ (z_{1-s}, \dots, z_{m-1}, z_m, \underbrace{0, \dots, 0}_{|s|}), & s < 0 \end{cases} \quad (5)$$

where $Z_{(s)}$ denotes the shifted sequence; s represents the shift step.

Table 2

Describes statistics of time delays of speed.

count	mean	std	min	25%	50%	75%	max
89	0	0	0	0	0	0	0

When all possible shifts $Z_{(s)}$ are considered, with $s \in [-m, m]$, we produce $CC_w(Z, Y) = (c_1, \dots, c_w)$, the cross-correlation sequence with length $2m - 1$, defined as follows:

$$CC_w(Z, Y) = R_{w-m}(Z, Y), w \in \{1, 2, \dots, 2m - 1\} \quad (6)$$

where $s = w - m$ and $R_{w-m}(Z, Y)$ is calculated as:

$$R_k(Z, Y) = \begin{cases} \sum_{l=1}^{m-k} z_{l+k} \cdot y_l, & k \geq 0 \\ R_{-k}(Y, Z), & k < 0 \end{cases} \quad (7)$$

Depending on the presence of errors in the original sequences, the coefficient normalization for $CC_w(X, Y)$ is required by dividing the cross-correlation sequence by the geometric mean of autocorrelations of the individual sequences, which are defined as follows:

$$NCC(Z, Y) = \frac{CC_w(Z, Y)}{\sqrt{R_0(Z, Z) * R_0(Y, Y)}} \quad (8)$$

After normalization of the sequence, we detect the position w where $NCC(Z, Y)$ is maximized, and we derive the following distance measure:

$$SBD(Z, Y) = 1 - \max_w (NCC(Z, Y)) \quad (9)$$

By determining the w corresponding to $SBD(Z, Y)$, the delay between the measured and actual sequences can be obtained, the required sensor delay.

Outlier detection: After calculating the sensor delay, outliers are caused due to device errors. One Class Support Vector Machine (OCSVM) is used in this paper to eliminate outliers. OCSVM is a natural extension of the support vector algorithm in the case of unlabeled data and functions well in outlier detection (Schölkopf et al., 1999). The strategy of this algorithm is to map the data into the feature space corresponding to the kernel and separate them from the origin with maximum margin. For a new point X , the functional value is determined by evaluating which side of the hyperplane it falls on in feature space. Via the freedom to utilize different types of kernel functions, this simple geometric picture corresponds to various nonlinear estimators in input space. For simplicity, we drop the specific algorithmic details of OCSVM found in the literature (Schölkopf et al., 2001, 2002).

3.2.2. Result analyses

Time delay of speed

The time delay of speed is obtained by applying the SBD algorithm to the actual speed calculated from the trajectory differential and the speed record in the experimental results. Fig. 3 indicates the time delay curve of speed with and without outlier detection, including 89 cases. Moreover, the statistical description of the pre-processed data is summarized in Table 2. The results of all 89 samples show that delay of speed is equal to 0 (at least less than the sampling period of 50ms).

Based on the above results, we can conclude that the time delay of speed is zero (at least much less than the sampling period of 50ms). This conclusion can be reasonably understood because of $\dot{x}_i = v_i = (Rr_{eff}\omega_e)_i$, where R is the gear ratio, r_{eff} is the effective tire radius, and ω_e is the engine speed. In cases where both R and r_{eff} are determined, v_i is positively correlated with ω_e which can be obtained easily and directly.

Time delay of gap

The time delay of gap is obtained by applying the SBD algorithm to the actual gap calculated from the trajectory difference between adjacent vehicles and the gap record in the experimental results. Fig. 4 shows the time delay curve

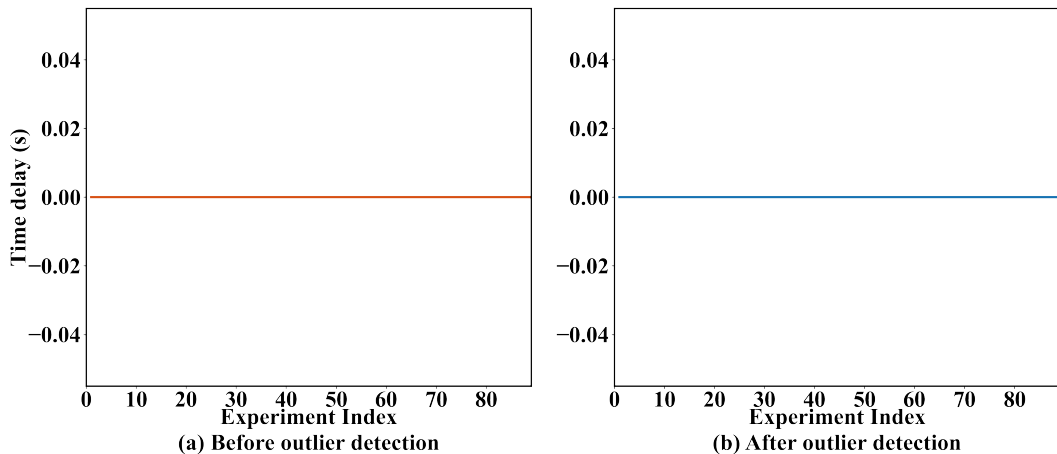


Figure 3: Time delays of speed in all experiment cases. (a) the time delays before outlier detection; (b) the time delays after outlier detection.

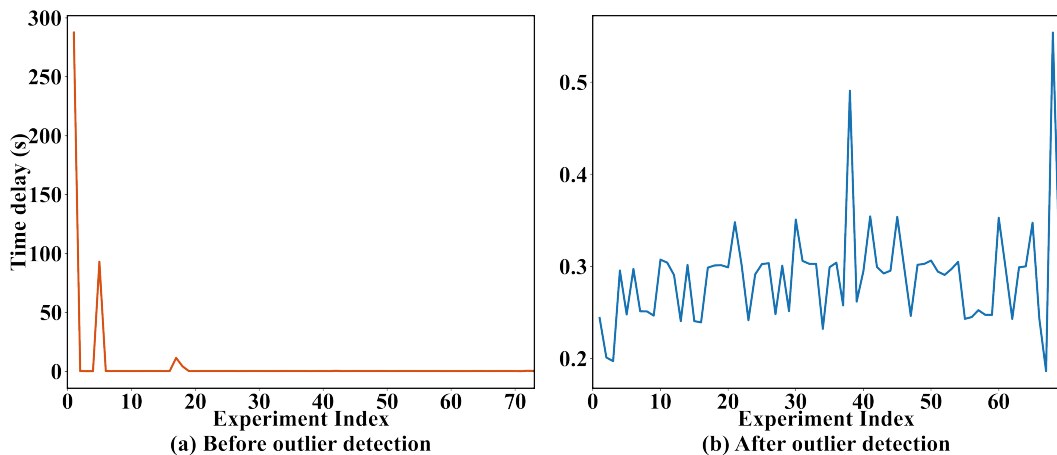


Figure 4: Time delays of gap in all experiment cases. (a) the time delays before outlier detection; (b) the time delays after outlier detection.

Table 3

Describes statistics of time delays of gap.

count	mean	std	min	25%	50%	75%	max
69	0.289097	0.055083	0.1863	0.2478	0.2973	0.3028	0.554

of gap with and without outlier detection, including 73 cases. Moreover, the statistical description of the pre-processed data is summarized in Table 3.

Time delay of lead speed

The time delay of lead speed is obtained by applying the SBD algorithm to the actual speed calculated from the trajectory differential of the predecessor and the lead speed record in the experimental results. Fig. 5 shows the time delay curve of lead speed with and without outlier detection, including 73 cases. Moreover, the statistical description of the pre-processed data is summarized in Table 4.

Validation of correlation between time delays

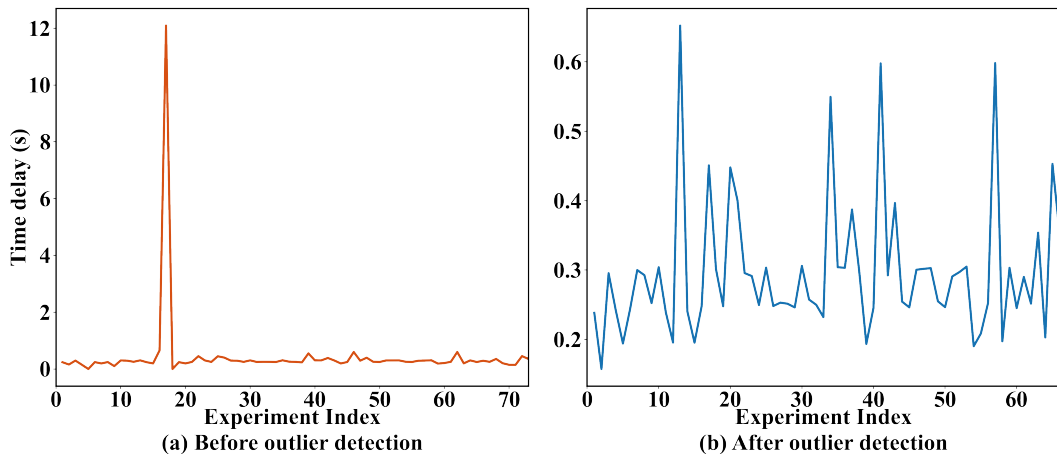


Figure 5: Time delays of lead speed in all experiment cases. (a) the time delays before outlier detection; (b) the time delays after outlier detection.

Table 4

Describes statistics of time delays of lead speed.

count	mean	std	min	25%	50%	75%	max
66	0.296894	0.098991	0.1575	0.245675	0.2738	0.30345	0.6523

Table 5

Results of Shapiro-Wilk test.

	Kolmogorov-Smirnov			Shapiro-Wilk		
	statistics	df	ρ	statistics	df	ρ
lead speed	0.168	64	0.000	0.946	64	0.007
gap	0.204	64	0.000	0.863	64	0.000

After obtaining the sensor delays of lead speed and gap, the correlation between the two needs to be analyzed to determine whether the sensor delays of different parameters are independent. A series of statistical hypothesis tests were performed based on the above reasons.

For the sake of selecting the hypothesis testing method, a normality test is conducted, and the corresponding test results are shown in Table 5. Take the results of Kolmogorov-Smirnov as an example, $\rho = 0.000 < 0.001$, which means that neither time delay of lead speed nor gap follows a normal distribution. The same conclusion can be drawn from the result of Shapiro-Wilk.

Since the time delays do not follow the normal distribution, the parametric tests do not apply to the problem. The Wageder-Samples Wilcoxon Signed-Rank test of Nonparametric tests was chosen to verify the differences between the two time delays. Table 6 presents the results of the Paired-Samples Wilcoxon Signed-Rank test. Since statistic $Z = -2.169$ and $\rho = 0.030 < 0.05$, the null hypothesis is rejected. Based on the above test results, we concluded a significant difference in time delays of lead speed and gap. In other words, the same parameter cannot represent the two from the perspective of statistics.

3.2.3. Result discussion

Based on the above analyses, several conclusions can be summarized for subsequent research:

1. The time delay of speed can be considered equal to 0 (much less than the sampling period of 50ms). Namely, it can be ignored in model modeling without affecting accuracy.

Table 6

Paired-Samples Wilcoxon Signed-Rank Test Statistics.

		gap-lead speed
Z		-2.169
Asymptotic Significance (2-tailed)		0.030

2. The time delays of lead speed and gap are statistically significantly different. Thus, different parameter representations must be chosen for each.

As a result, Equation(2) can be rewritten to the following form without losing accuracy:

$$u_i(t) = f(s_i(t - \eta_s), v_i(t), v_{i-1}(t - \eta_{fv})) \quad (10)$$

3.3. Lower controller

3.3.1. System identification methods

Method: For the case of the lower level controller, transfer relationships between the input signal of command acceleration and the output signal of actual acceleration are urgent to be determined. To characterize the transfer relationships between inputs and outputs, a mathematical function is known as the transfer function that theoretically models the output for each possible input is chosen. The above problem is also known as the system identification problem. The algorithm in system identification can be summarized as (Ozdemir and Gumussoy, 2017; Kollár et al., 2006; Ljung, 1995):

1. Map s domain to q via $q(s) = \frac{\alpha+s}{\alpha-s}$;
2. Scale measurements H_i ;
3. Initial fit: Use monomial basis with $d^{(0)}(q) = 1$;
4. Sanathanan-Koerner (SK) iterations: Use orthonormal rational polynomial basis functions on the unit disk. Iterate until the maximum number of iterations or convergence. Update basis functions at each step;
5. Instrumental Variable (IV) iterations: Use the final set basis functions used in SK iterations. Iterate until the maximum number of iterations or convergence;
6. Use the best solution found for the nonlinear least-squares problem throughout all steps (initial fit, SK, and IV iterations). Calculate the corresponding zero-pole-gain model;
7. Revert s to q domain mapping via $s = \frac{\alpha(q-1)}{q+1}$;
8. Revert measurement scaling;
9. Convert zero-pole-gain to transfer function model.

Data preparation: The commanded acceleration and actual acceleration of each ACC are extracted from the field experiment and paired one by one. Then divide all data (89 cases) into working data (70 cases) for transfer function estimation and validation data (19 cases) for validation. Moreover, the working data is further grouped into 7 batches of 10 cases each.

3.3.2. Result analyses

Applying the aforementioned method to the prepared data, the system identification results in the form of Equation(3) and Equation(4) are obtained:

$$G_i(s) = \frac{k_G}{\tau_i s + 1} = \frac{0.93430}{0.9749s + 1} \quad (11)$$

$$G_i(s) = \frac{k_G}{\tau_i s + 1} e^{-\phi_i s} = \frac{0.98892}{0.7148s + 1} e^{-0.2s} \quad (12)$$

For the results in Equation(11) and Equation(12), the estimated evaluation indicators FPE (Akaike's Final Prediction Error) and MSE (Mean Square Error) are presented in Table 6. We find that cases where the actuator delay

Table 7

Comparison of different form on the estimated evaluation indicators FPE and MSE.

FPE	MSE							
	1st	2nd	3rd	4th	5th	6th	7th	
With actuator delay	0.1463	0.1636	0.1216	0.1298	0.1298	0.1388	0.1611	0.1820
Without actuator delay	0.1972	0.2300	0.1672	0.1747	0.1747	0.1827	0.2167	0.2407

is introduced can reduce the FPE by 25.81% compared to what is not introduced. Moreover, the MSE of the case with actuator delay can be significantly reduced compared to the case without in each batch, and the average reduction rate of 7 batches is 25.95%.

The caveat is that the fitting results of the lower level controller models of EVs and gasoline vehicles may be different, so the model fitting results based on the data of different vehicles in Appendix 5 have also been presented in detail.

In summary, we can conclude that introducing the actuator lag can effectively improve the model fit. Therefore, Equation(4) compared to Equation(3) can accurately describe the transfer relationship between the input and output of the lower level controller.

4. Stability analyses

The previous sections propose and validate the hierarchical control model of the ACC based on field data. This section further explores the local stability and string stability characteristics under the hierarchical control model.

4.1. Vehicle longitudinal dynamic model

A vehicle longitudinal dynamic model mainly consists of the engine, throttle and brake actuators, drive train, transmission, and torque converter. Under a variety of resistance forces, the longitudinal dynamics of vehicle i can be modeled by the following force balance equation:

$$m_i a_i(t) = f_i^e(t) - f_i^g(t) - f_i^w(t) - f_i^r(t) \quad (13)$$

where m_i stands for the unknown mass of vehicle i ; $f_i^e(t)$ is the desired engine force acting on vehicle i ; $f_i^g(t)$, $f_i^w(t)$, and $f_i^r(t)$ denote the gravity component parallel to the road surface, air resistance force, and rolling resistance force, respectively.

The functions of the lumped uncertain resistance forces, including $f_i^g(t)$, $f_i^w(t)$, and $f_i^r(t)$ are expressed as follows:

$$\begin{cases} f_i^g(t) = m_i g \sin(\theta_i(t)) \\ f_i^w(t) = \frac{1}{2} \rho C_D A_F (v_i(t) + v_w(t))^2 \\ f_i^r(t) = \mu_R m_i g \cos(\theta_i(t)) \end{cases} \quad (14)$$

where $g = 9.81 m/s^2$ denotes the acceleration of gravity; $\theta_i(t)$ is the inclination angle of the road; ρ denotes the air density; C_D is the aerodynamic drag coefficient; A_F represents the maximal cross-sectional/frontal area of the vehicle; $v_w(t)$ denotes the uncertain headwind speed; μ_R is the coefficient of rolling resistance.

From designing a control strategy, a nonlinear vehicle dynamic model is obviously not suitable due to its nonlinear characteristics. Fortunately, by adopting nonlinear state feedback, it can be transformed into a linearized model to keep the characteristics of the Driveline dynamics while reducing the negative effects caused by nonlinear characteristics at the linear level.

According to the lower level controller in Equation(4), the engine dynamic is modeled as follows:

$$\tau_i s + 1) F_i^e = k_G e^{-\phi_i s} U_i \quad (15)$$

Adopting the inverse Laplace transformation on Equation(15) arrives at:

$$\dot{f}_i^e(t) = \frac{k_G u_i(t - \phi_i)}{\tau_i} - \frac{f_i^e(t)}{\tau_i} \quad (16)$$

Substituting Equation(13) into Equation(16) and differentiating both sides of Equation(16) with respect to time, we get:

$$\begin{aligned}\dot{a}_i(t) &= \frac{\dot{f}_i^e(t)}{m_i} - \frac{\dot{f}_i^g(t)}{m_i} - \frac{\dot{f}_i^w(t)}{m_i} - \frac{\dot{f}_i^r(t)}{m_i} \\ &= \frac{k_G u_i(t - \phi_i)}{m_i \tau_i} - \frac{a_i(t) + g \sin(\theta_i(t)) [1 - \tau_i \mu_R \dot{\theta}_i(t)] + g \cos(\theta_i(t)) [1 + \tau_i \dot{\theta}_i(t)]}{\tau_i} \\ &\quad - \frac{\frac{1}{2} \rho C_D A_F (v_i(t) + v_w(t)) ((v_i(t) + v_w(t)) + 2\tau_i(a_i(t) + \dot{v}_w(t)))}{\tau_i}\end{aligned}\quad (17)$$

Thus, the nonlinear state feedback chosen for linearizing can be defined by:

$$\begin{aligned}u_i^*(t) &= k_G m_i u_i(t - \phi_i) + g \sin(\theta_i(t)) [1 - \tau_i \mu_R \dot{\theta}_i(t)] + g \cos(\theta_i(t)) [1 + \tau_i \dot{\theta}_i(t)] \\ &\quad + \frac{1}{2} \rho C_D A_F (v_i(t) + v_w(t)) ((v_i(t) + v_w(t)) + 2\tau_i(a_i(t) + \dot{v}_w(t)))\end{aligned}\quad (18)$$

The linear differential equations for the lower level controller can be rewritten as:

$$\tau_i \dot{a}_i(t) + a_i(t) = u_i(t - \phi_i)\quad (19)$$

4.2. Error transfer function

An error transfer function needs to be proposed for the stability analysis below to provide a systematic theoretical analysis. It is worth mentioning that exogenous disturbances in both speed and gap can be regarded as signals to determine stability in the literature (Feng et al., 2019; Qin et al., 2018; Navas and Milanés, 2019; Jin and Orosz, 2014). For a homogeneous traffic flow, the same stability conditions can be derived based on speed and gap disturbances (Montanino et al., 2021; Montanino and Punzo, 2021; Zheng et al., 2015). However, the case based on speed disturbances can provide a more concise derivation. Therefore, we take speed disturbances as the signal to determine stability.

The primary control objective for the ACC is to track the predecessor, so we assume the ACC is under the equilibrium state when subjecting to exogenous disturbances. The aforementioned assumption holds when the following two conditions are met:

1. the ACC system is satisfied with local stability, that is, it can satisfy $\lim_{t \rightarrow \infty} |f(s_i(t - \eta_s), v_i(t), v_{i-1}(t - \eta_{fv}))| = 0$;
2. the frequency of disturbances is small enough to ensure that the ACC can recover to the equilibrium state from the latest disturbance.

For the former, local stability is a basic requirement that commercial ACCs must meet to achieve their control objectives. And for the latter, the disturbances faced generally do not have periodicity and are considered infinitely long periods in actual traffic scenarios (Bian et al., 2019; Xiao and Gao, 2011).

In the equilibrium state, the vehicle speed in the traffic flow is equal to the equilibrium state speed v_e , the speed difference between adjacent vehicles is zero, the car-following gap between the vehicles maintains the desired gap s_e and the acceleration of the vehicle is zero:

$$\begin{cases} v_n = v_{n-1} = v_n^e \\ s_n = s_n^e \\ f(s_n^e, v_n^e, v_n^e) = 0 \end{cases}\quad (20)$$

First, linearize the upper controller Equation(10) at the equilibrium state:

$$f(s_i(t - \eta_s), v_i(t), v_{i-1}(t - \eta_{fv})) \approx f_{si} \hat{s}_i(t - \eta_s) + f_{vi} \hat{v}_i(t) + f_{vi-1} \hat{v}_{i-1}(t - \eta_{fv})\quad (21)$$

where $\hat{s}_i = s_i - s_e$, $\hat{v}_i = v_i - v_e$, and $\hat{v}_{i-1} = v_{i-1} - v_e$ represent the small deviation of the gap, speed, and lead speed around the equilibrium state, respectively; $f_{si} = \left. \frac{\partial f}{\partial v_i} \right|_{(s_e, v_e)}$, $f_{vi} = \left. \frac{\partial f}{\partial v_i} \right|_{(s_e, v_e)}$, and $f_{vi-1} = \left. \frac{\partial f}{\partial v_{i-1}} \right|_{(s_e, v_e)}$ is the partial differential equations for gap, speed, and lead speed.

Inserting the lower level controller Equation(19) into the linearized upper controller Equation(21) yields that:

$$\tau_i \ddot{a}_i(t) + a_i(t) = f_{si} \hat{s}_i(t - \eta_s - \phi_i) + f_{vi} \hat{v}_i(t - \phi_i) + f_{v_{i-1}} \hat{v}_{i-1}(t - \eta_{fv} - \phi_i) \quad (22)$$

Then, calculating the time derivative of Equation(22) arrives at:

$$\tau_i \ddot{a}_i(t) + \dot{a}_i(t) = f_{si} (\hat{v}_{i-1}(t - \eta_s - \phi_i) - \hat{v}_i(t - \eta_s - \phi_i)) + f_{vi} a_i(t - \phi_i) + f_{v_{i-1}} a_{i-1}(t - \eta_{fv} - \phi_i) \quad (23)$$

Performing Laplace transform, assuming the homogeneous vehicle platoon and zero initial conditions, the transfer function relating the speed errors of consecutive vehicles in the platoon can be written by:

$$G_i(s) = \frac{V_i(s)}{V_{i-1}(s)} = \frac{f_{si} e^{-\eta_s^* s} + f_{fv} e^{-\eta_{fv}^* s}}{\tau_i s^3 + s^2 + f_{si} e^{-\eta_s^* s} - f_{v_i} e^{-\eta_v^* s}} \quad (24)$$

where $\eta_s^* = \eta_s + \phi_i$, $\eta_{fv}^* = \eta_{fv} + \phi_i$, $\eta_v^* = \phi_i$, $f_{fv} = f_{v_{i-1}}$ for brevity.

4.3. String stability analyses

4.3.1. Definition

Before the string stability analyses, the definition of string stability discussed in this paper needed to be clarified because it varies in literature (Wilson, 2008; Treiber and Kesting, 2011; Ruan et al., 2021). Namely, the exogenous disturbance will not be amplified during upstream propagation (Montanino and Punzo, 2021; Qin and Wang, 2021; Jin and Orosz, 2014), i.e., for every vehicle i , the ∞ norm of the error signal is not greater than that of its predecessor, satisfied:

$$\|e_i\|_\infty \leq \|e_{i-1}\|_\infty \quad (25)$$

However, the Euclidean norm is easier to control the analysis and design of the system than the infinite norm. Therefore, by introducing the impulse response of the transfer function, Equation(25) can be replaced by the two conditions (Swaroop, 1994; Darbha and Rajagopal, 1999):

$$\|G(s)\|_\infty = \sup \frac{\|e_i\|_2}{\|e_{i-1}\|_2} \leq 1 \text{ and } g(t) > 0 \quad (26)$$

where $g(t)$ denotes the impulse response of the transfer function $G(s)$.

The condition $g(t) > 0$ can be easily satisfied by designing a compensator (Rajamani, 2011; Darbha, 2003). $g(t) > 0$ ensures that steady state of e_i and e_{i-1} have the same sign. Otherwise, it would be dangerous even if $\|G(s)\|_\infty \leq 1$ is satisfied.

4.3.2. String stability criterion

Converting from S-domain to the frequency domain by substituting $s = j\omega$ into the transfer function Equation(24) arrives at:

$$\begin{cases} G_i(j\omega) = \frac{R_i(j\omega)}{D_i(j\omega)} \\ R_i(j\omega) = f_{si} (\cos(\omega\eta_s^*) - j \sin(\omega\eta_s^*)) + f_{fv} (j\omega \cos(\omega\eta_{fv}^*) + \omega \sin(\omega\eta_{fv}^*)) \\ D_i(j\omega) = -j\tau_i\omega^3 - \omega^2 + f_{si} (\cos(\omega\eta_s^*) - j \sin(\omega\eta_s^*)) - f_{v_i} (j\omega \cos(\omega\eta_v^*) + \omega \sin(\omega\eta_v^*)) \end{cases} \quad (27)$$

To satisfy the string stability condition $\|G(s)\|_\infty \leq 1$, calculating the modulo of the above fraction and squaring it, we get:

$$\begin{cases} |R_i|^2 = f_{si}^2 + \omega^2 f_{fv}^2 + 2\omega f_{si} f_{fv} \sin(\omega(\eta_{fv}^* - \eta_s^*)) \\ |D_i|^2 = \tau_i^2 \omega^6 + \omega^4 + f_{si}^2 + \omega^2 f_{v_i}^2 + 2\omega f_{si} f_{v_i} \sin(\omega(\eta_s^* - \eta_v^*)) - \omega^2 f_{fv}^2 \\ \quad + 2\omega^2 [f_{si} (\tau_i \omega \sin(\omega\eta_s^*) - \cos(\omega\eta_s^*)) + \omega f_{v_i} (\tau_i \omega \cos(\omega\eta_v^*) + \sin(\omega\eta_v^*))] \end{cases} \quad (28)$$

With the equivalence relationship: $\| G(s) \|_{\infty} \leq 1 \iff \frac{|R_i|^2}{|D_i|^2} \leq 1$, the string stability is unconditionally satisfied if:

$$|D_i|^2 - |R_i|^2 \geq 0 \quad (29)$$

Inserting Equation(28) into Equation(29) yields that:

$$\begin{aligned} & \tau_i^2 \omega^6 + \omega^4 + 2\omega f_{s_i} f_{v_i} \sin(\omega(\eta_s^* - \eta_v^*)) - 2\omega f_{s_i} f_{fv} \sin(\omega(\eta_{fv}^* - \eta_s^*)) - \omega^2 f_{fv}^2 \\ & + \omega^2 f_{v_i}^2 + 2\omega^2 [f_{s_i} (\tau_i \omega \sin(\omega \eta_s^*) - \cos(\omega \eta_s^*)) + \omega f_{v_i} (\tau_i \omega \cos(\omega \eta_v^*) + \sin(\omega \eta_v^*))] \geq 0 \end{aligned} \quad (30)$$

Applying a linear approximation based on the assumption that the frequency of disturbance is approximately 0, e.g. $\lim_{x \rightarrow 0} \sin x = x$ and $\lim_{x \rightarrow 0} \cos x = 1$, the Equation(30) can be rewritten as:

$$\begin{aligned} & \tau_i^2 \omega^6 + \omega^4 + 2\omega^2 f_{s_i} f_{v_i} (\eta_s^* - \eta_v^*) - 2\omega^2 f_{s_i} f_{fv} (\eta_{fv}^* - \eta_s^*) - \omega^2 f_{fv}^2 \\ & + \omega^2 f_{v_i}^2 + 2\omega^2 [f_{s_i} (\tau_i \omega^2 \eta_s^* - 1) + \omega f_{v_i} (\tau_i \omega + \omega \eta_v^*)] \geq 0 \end{aligned} \quad (31)$$

Rearranging the coefficient of the inequality Equation(31), the string stability is guaranteed if and only if:

$$\left\{ \begin{array}{l} C_6 \omega^6 + C_4 \omega^4 + C_2 \omega^2 \geq 0, \forall \omega \in (0, +\infty) \\ C_6 = \tau_i^2 \\ C_4 = 1 + 2f_{s_i} \tau_i \eta_s^* + 2f_{v_i} (\tau_i + \eta_v^*) \\ C_2 = 2f_{s_i} f_{v_i} (\eta_s^* - \eta_v^*) + f_{v_i}^2 - 2f_{s_i} f_{fv} (\eta_{fv}^* - \eta_s^*) - 2f_{s_i} - f_{fv}^2 \end{array} \right. \quad (32)$$

Based on the inequality in Equation(32), string stability is guaranteed if either of the following two conditions is satisfied:

1. string stability condition I: $C_4 > 0, C_2 > 0$;
2. string stability condition II: $\Delta = C_4^2 - 4C_2C_6 < 0$.

Notice, since the $C_6 = \tau_i^2 > 0$, the corresponding constraints are omitted but without loss of generality. Stability condition I indicates the case that the inequality has no roots or is rooted in the left half-plane of the x-axis to ensure that the inequality is always greater than zero for $\forall \omega \in (0, +\infty)$. As for stability condition II, it illustrates the case where inequality does not have any root. It is worth mentioning that stability condition I and stability condition II are both sufficient and unnecessary conditions for string stability, so they do not have to be satisfied at the same time to ensure string stability.

In the remainder of this section, we will take practical ACC control strategies as an example to explore the applicability of the above theoretical analysis.

4.3.3. Analyses of string stability based on example ACC

To analyze the actual stability conditions, here we consider the well-known linear ACC control strategy, namely constant time gap (CTG), for example:

$$u_i(t) = f(s_i(t - \eta_s), v_i(t), v_{i-1}(t - \eta_{fv})) = k_g (s_i(t - \eta_s) - v_i(t) T_g) + k_v (v_{i-1}(t - \eta_{fv}) - v_i(t)) \quad (33)$$

where k_g and k_v are the feedback gains on gap error and speed error, respectively.

The partial derivatives of Equation(33) are given by:

$$\left\{ \begin{array}{l} f_{s_i} = k_g \\ f_{v_i} = -k_g T_g - k_v \\ f_{fv} = k_v \end{array} \right. \quad (34)$$

Table 8

Chosen value of the other parameters except for the control parameters.

Parameter	τ_i	ϕ_i	η_s	η_v	η_{fv}
Value	0.7148s	0.2s	0.2891s	0s	0.2969s

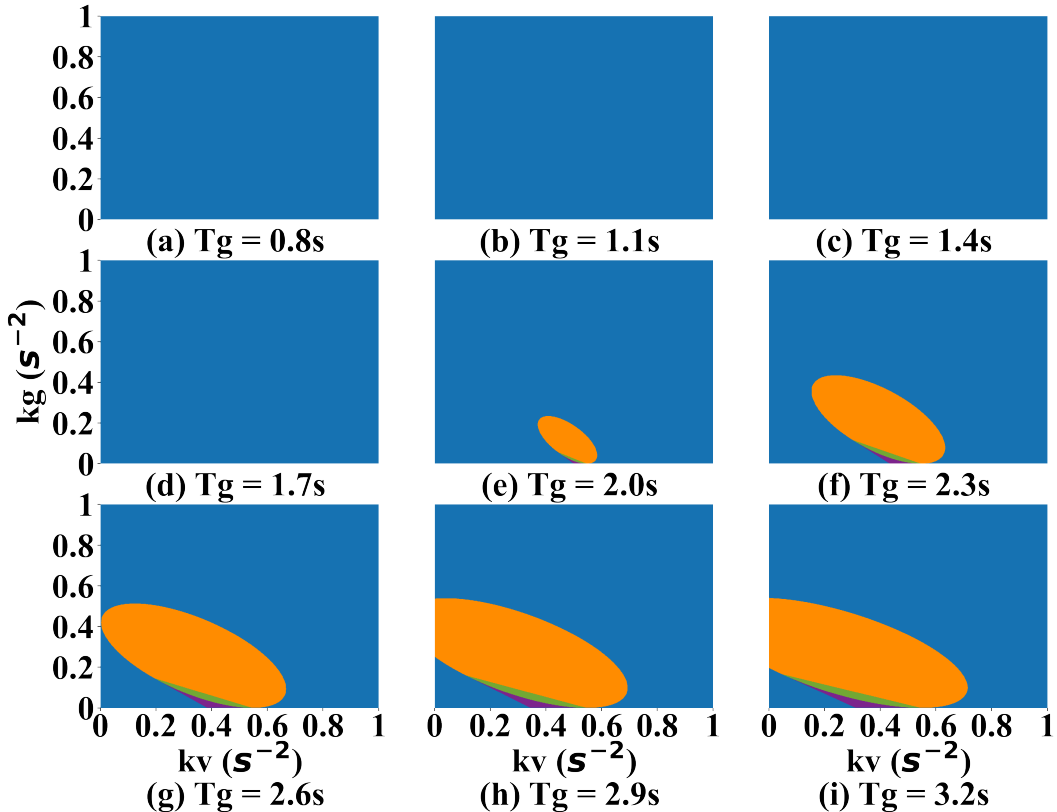


Figure 6: Stability diagram in the space $(k_g - k_v)$ under different desired time gap T_g , where purple region depicts the stability region under stability type I; orange region depicts stability type II; green region depicts both satisfied type I and II; blue region depicts instability.

Substituting Equation(34) into Equation(33) arrives at:

$$\begin{cases} C_6\omega^6 + C_4\omega^4 + C_2\omega^2 \geq 0, \forall \Omega \in (0, +\infty) \\ C_6 = \tau_i^2 \\ C_4 = 1 + 2k_g\tau_i\eta_s^* - 2(k_gT_g + k_v)(\tau_i + \eta_v^*) \\ C_2 = -2k_g(k_gT_g + k_v)(\eta_s^* - \eta_v^*) - 2k_gk_v(\eta_{fv}^* - \eta_s^*) - 2k_g + (k_gT_g + k_v)^2 - k_v^2 \end{cases} \quad (35)$$

4.3.4. Sensitivity analyses

Based on the stability parameter Equation(35) and stability conditions, the sensitivity of control parameters (k_g, k_v, T_g) on string stability can be explored. Table 8 presents the chosen value of the other parameters except for the control parameters in the sensitivity analyses. Moreover, Fig. 6 illustrates the stability diagram in the space $(k_g - k_v)$ under different desired time gap T_g , where purple region depicts the stability region under stability type I; orange region depicts stability type II; green region depicts both satisfied type I and II; blue region depicts instability.

From Fig. 6, one conclusion that can be concluded is that if the T_g is less than 1.7s, ACC cannot maintain string stability regardless of how other control parameters are chosen. For T_g greater than 1.7s, the stable region can be significantly increased in the space $(k_g - k_v)$ as the T_g increases. However, even $T_g = 3.2s$, ACC can maintain string stability only in cases where the control parameters are small, which means the response to changes caused by disturbances is relatively slow. That is, it is poor system responsiveness. In another perspective, when the control parameters are set to approach 0, the stability condition II becomes hard to achieve, which will cause the ACC to become unstable. In addition, by comparing the stability regions corresponding to different stability conditions, it can be found that stability condition II is easier to satisfy than stability condition I and that the boundary between stability condition I and II will be shifted as the T_g increases.

In Appendix 5, sensitivity analysis of different device parameters is discussed. An additional conclusion that can be concluded is that effective control of the delay in the lower level controller can significantly enlarge the stability region.

4.3.5. Experiment validation

Based on the theoretical results of the stability analysis in Section 4.3.4, the corresponding field experiments need to be conducted to verify the above conclusions. However, due to the limitations of the experimental field and funds, the experiments in the fully stable region are not realistic, and the cost is difficult to afford. Therefore, we use the experimental data obtained in Section 3 to verify theoretical results partially. Fig. 7 presents the speed curve of each vehicle in each experiment round. Moreover, the subgraph order corresponds to the index in Table 1. It should be noted that due to device errors, the data of the third car in the first round and fifth round are not shown, but the impact on the experimental verification results can be ignored.

Fig. 7 shows the case where only subgraphs (a) and (b) guarantee string stability while others else do not. This phenomenon conforms to the results of theoretical analysis in Section 4.3.4 since only the control parameter settings for (a) and (b) are included in the stability region in Fig. 6. It is worth noting that theoretical results can only be partially verified through field data, which is limited by the development of field experiments.

5. Conclusion and future work

The paper developed a general hierarchical control system consisting of an upper level controller and a lower level controller to model the ACC system. In the upper level controller model, an assumption is proposed that different parameters have different perception time delays based on device characteristics. For the case of the lower level controller model, the existing assumptions are meliorated to make them fit the field data more. Besides, field experiments were conducted, and corresponding field data verified that the general hierarchical system could model the ACC system more accurately than the traditional system. In addition, the frequency-based linear string stability method is applied to derive the string stability condition under the general hierarchical control system. An ACC example under CTG control strategies was chosen to explore the stable regions under different control parameters for giving new insights into the relationship between the string stability properties of the system properties of time delays and controller design parameters of feedback gains and desired time gap. Moreover, the theoretical analysis results were partially verified based on field data. Last but not least, this paper explored the direction of string stability optimization to guide further research.

We need to acknowledge that the lower level controller model proposed above is still a fitted model despite maintaining a higher fitness with the field data. An improved lower level controller model that can balance fit and complexity needs to be proposed to provide a model basis for further ACC research. In addition, existing string stability analyses only target homogeneous ACC traffic flows, and the string stability conditions of the corresponding heterogeneous traffic flow being ACC-MV and ACC-MV-CACC need to be further studied to serve the application of this technology. Another problem is that the amount of data used in this study cannot be called sufficient due to the difficulty and cost of field experiments. Future research also tends to conduct more field experiments to expand the database further.

Appendix A. Detailed information of experimental vehicles

The detailed information of six experimental vehicles including make and model, size, and swept volume are shown in Table 9.

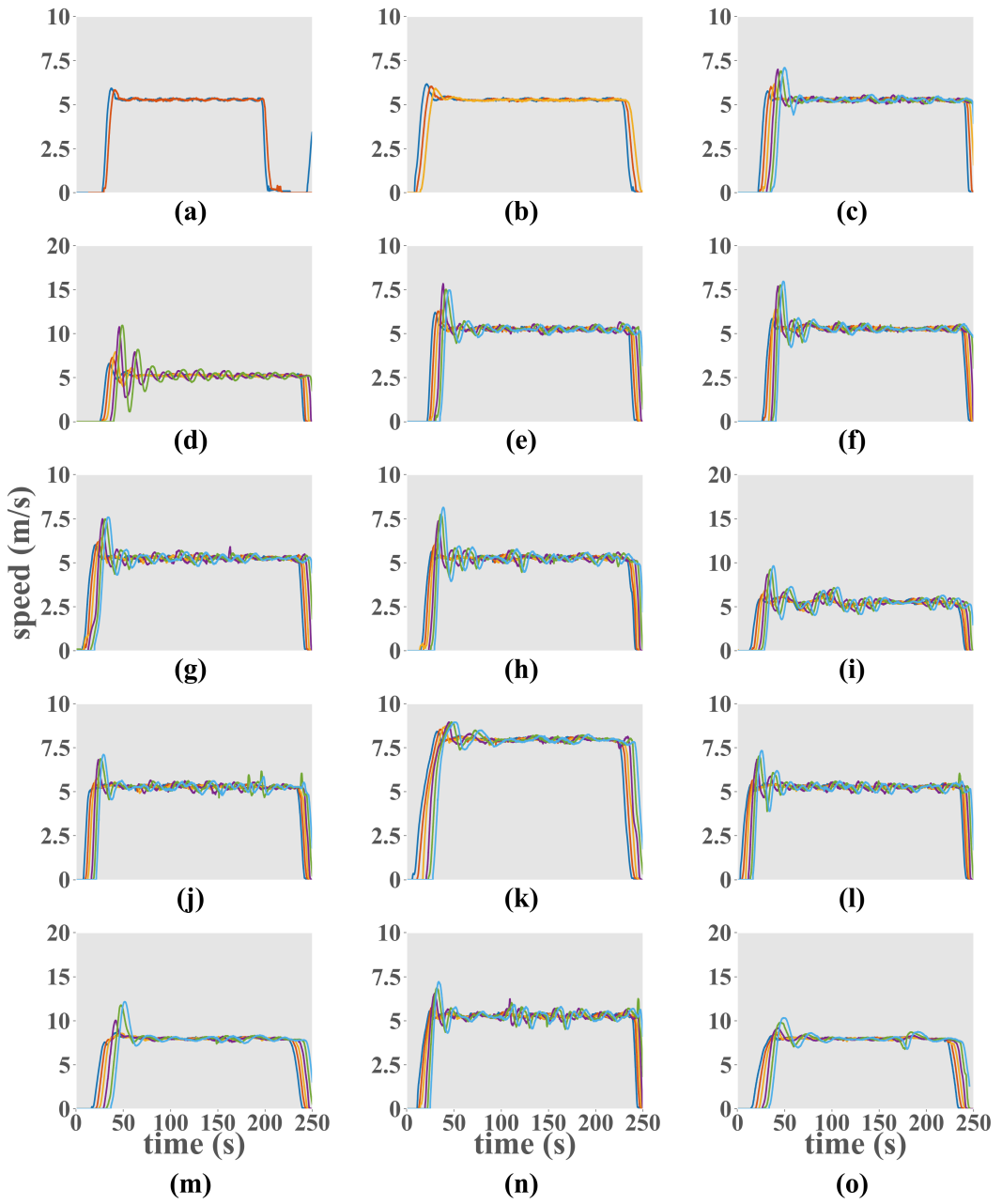


Figure 7: The speed curve of each vehicle in each experiment.

Appendix B. Model fitting results based on the data of different vehicles

The model fitting results with/without actuator delay based on the data of each experiment vehicle are shown in Table 10.

Appendix C. Sensitivity analysis of different device parameters

In this appendix, the impact of device parameters on the stability region is explored, including τ_i , ϕ_i , η_s , η_v , and η_{fv} . In order to further differentiate the difference between the values of device parameters, here we select $T_g = 3.2s$

Table 9

The detail information of experimental vehicles.

Vehicle index	Make and mode	$L \times W \times H(\text{mm} \times \text{mm} \times \text{mm})$	Swept volume (L)
1	CHANGAN AUTO CS55 E-Rocks	4515 × 1860 × 1690	EV
2	CHANGAN AUTO CS55 PLUS	4515 × 1865 × 1680	1.5
3	BAIC MOTOR ARCFOX αT	4788 × 1940 × 1683	EV
4	CHANGAN AUTO CS55 E-Rocks	4515 × 1860 × 1690	EV
5	CHANGAN AUTO CS55 E-Rocks	4515 × 1860 × 1690	EV
6	CHANGAN AUTO CS55 E-Rocks	4515 × 1860 × 1690	EV

* Electric Vehicle is abbreviated as EV.

Table 10

Model fitting results based on the data of different vehicles.

	Vehicle 1	Vehicle 2	Vehicle 3	Vehicle 4	Vehicle 5	Vehicle 6
	MSE	MSE	MSE	MSE	MSE	MSE
With actuator delay	0.1333	0.1544	0.1449	0.1486	0.1776	0.1511
Without actuator delay	0.1357	0.1751	0.1614	0.1801	0.2031	0.1980

for comparison. It is worth mentioning that the other device parameters are fixed in the case of any device parameter, and the parameters settings are shown in Table 8.

C.1 The case of τ_i

For studying the impacts of different τ_i on the stability region, here we select $\tau_i = 0.2, 0.4, 0.6, 0.7148\text{s}$ to explore, of which $\tau_i = 0.7148\text{s}$ is used as the benchmark scheme for comparison. Fig. 8 presents the stability region in the space $(k_g - k_v)$ under different τ_i .

Fig. 8 demonstrates one conclusion is that by inhibiting τ_i can significantly enlarge the stability region. Focusing on the stability region guaranteed by different stability conditions, another phenomenon can be found. The area of the stability region that satisfies stability condition I is significantly expanded compared to that of the stability region that meets stability condition II with the decrease of τ_i .

C.2 The case of ϕ_i

For further exploring the impacts of different ϕ_i on the stability region, four-parameter values are chosen as the contrast schemes, respectively being $\phi_i = 0.1, 0.2, 0.3, 0.4\text{s}$. The caveat is that $\phi_i = 0.2\text{s}$ is chosen as the baseline scheme because of its same value as the parameter calibration. Fig. 9 presents the stability region in the space $(k_g - k_v)$ under different ϕ_i .

Fig. 9 shows a similar conclusion to Fig. 8 that the stability region can be significantly expanded by suppressing ϕ_i . However, the two function to enlarge the stability region based on different reasons. For this case, it is mainly by expanding the area of the stability region under stability condition II with the decrease of ϕ_i .

C.3 The case of η_s

As for the impacts of different η_s on the stability region, $\eta_s = 0.1, 0.2, 0.2891, 0.4\text{s}$ are chosen to explore specifically. In this case, $\eta_s = 0.2891\text{s}$ is the baseline for the comparison as it is the same as the original case. Fig. 10 presents the stability region in the space $(k_g - k_v)$ under different η_s .

Fig. 10 illustrates a diametrically opposed phenomenon compared to the aforementioned two cases that the stability region is shrinking as the η_s decreasing. This is counterintuitive because we generally regard the perception delay of the device as a factor that undermines the stability of the system. Nevertheless, this phenomenon can be comprehended that the response time of the system is long enough to complete the response to disturbances due to the delay in the perception of the spacing. Therefore, suppressing the infinite norm amplitude of the response to guarantee the string stability. Another thing needed to be emphasized is that varieties in η_s have less impact on the stability region than

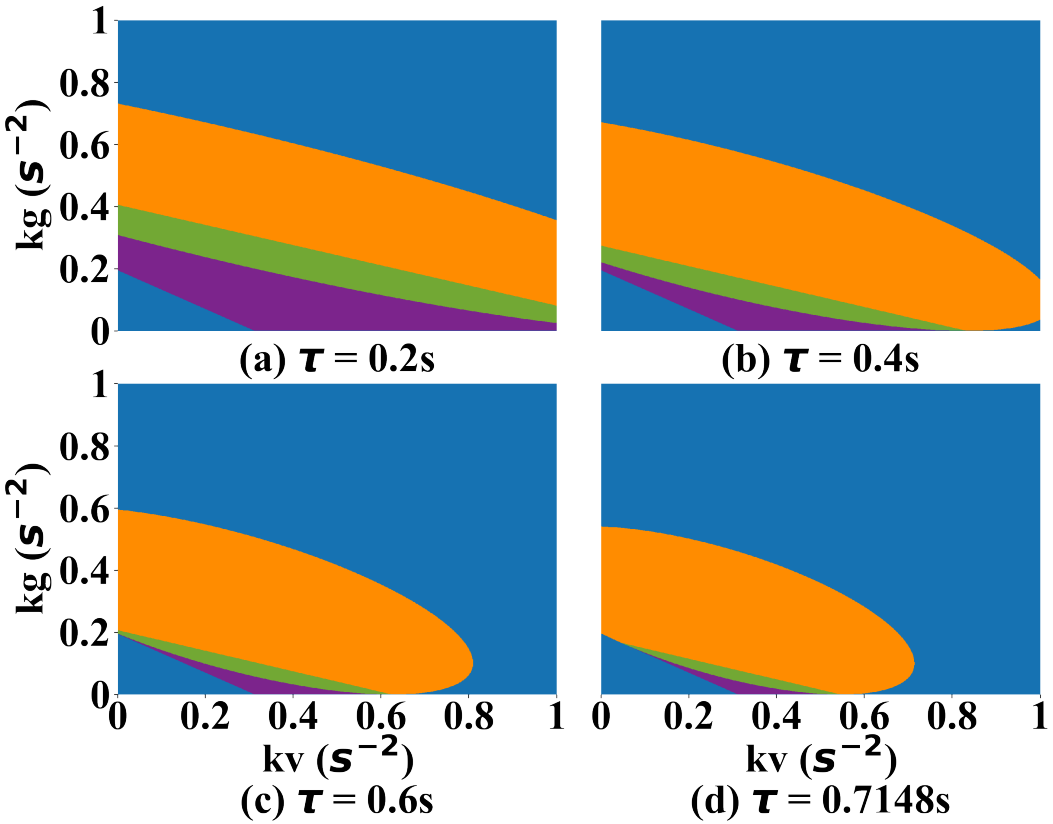


Figure 8: Stability diagram in the space $(k_g - k_v)$ under different τ_i , where purple region depicts the stability region under stability type I; orange region depicts stability type II; green region depicts both satisfied type I and II; blue region depicts instability.

in the first two cases. Based on this finding, optimization of the stability region should focus more on other device parameters than on η_s

C.4 The case of η_v

In the case of η_v , $\eta_v = 0, 0.1, 0.2, 0.3s$ are chosen to explore specifically. In this case, $\eta_v = 0s$ is the baseline for the comparison as it is the same as the original case. Fig. 11 presents the stability region in the space $(k_g - k_v)$ under different η_v .

A similar conclusion can be drawn that string stability deteriorates with η_v increasing from Fig. 11. Unlike the first two cases, the η_v is considered close to 0 based on field data, which means it does not require further optimization for this parameter. Therefore, in the process of improving the string stability of the ACC system, the perception devices of the speed can be ignored.

C.5 The case of η_{fv}

As for η_{fv} , similar parameter settings are the same as η_s have been chosen that $\eta_{fv} = 0.1, 0.2, 0.2969, 0.4s$ to explore the effect of the changes in η_{fv} on the stability region, not only increasing but decreasing. As the same, $\eta_{fv} = 0.2969s$ is regarded as the baseline to compare stability regions under parameter changes. Fig. 12 presents the stability region in the space $(k_g - k_v)$ under different η_{fv} .

Fig. 12 demonstrates that there is remarkably little variation in the stability region with the change of η_{fv} . This phenomenon is rational since only C_2 of the coefficients of Equation(35) related to η_{fv} . Moreover, η_{fv} only functions in the part of its difference from η_s , which further limits the impact of its changes.

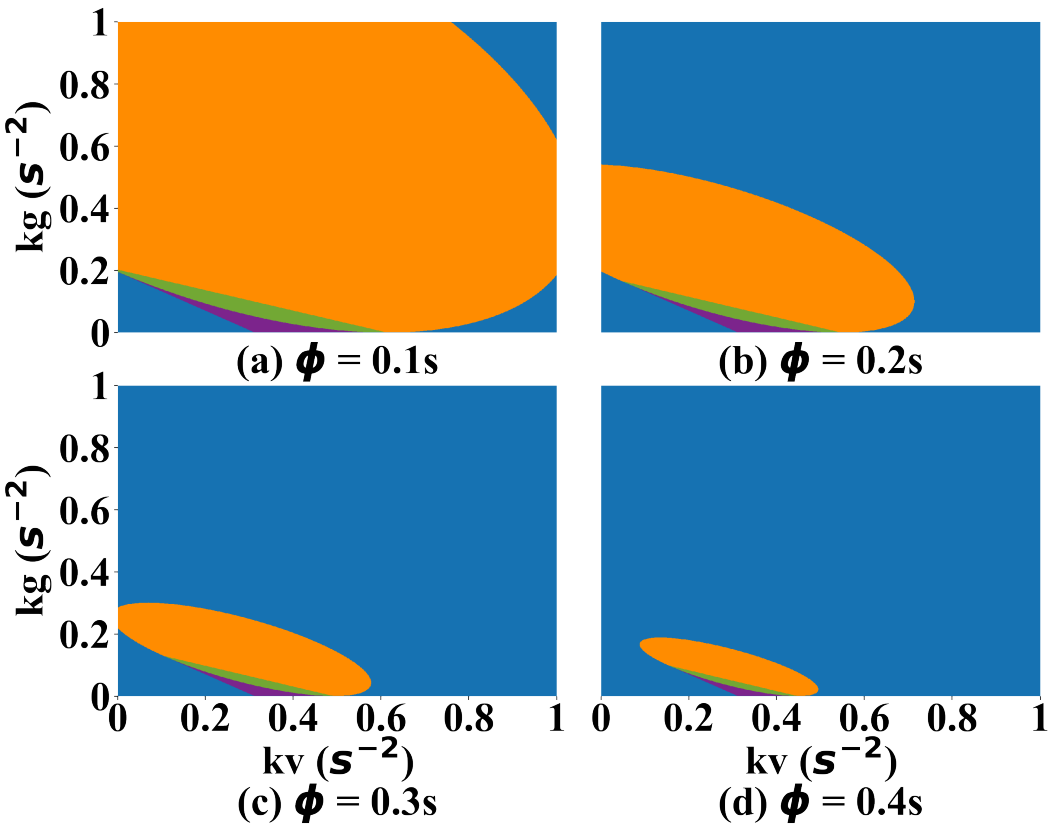


Figure 9: Stability diagram in the space $(k_g - k_v)$ under different ϕ_i , where purple region depicts the stability region under stability type I; orange region depicts stability type II; green region depicts both satisfied type I and II; blue region depicts instability.

C.6 Brief summary

For device parameters in the upper level controller, including η_s , η_v , and η_{fv} , optimizing them is not effective for improving the string stability of the ACC system. However, for device parameters in the lower-level controller, including τ_i and ϕ_i , the string stability region of the ACC system can be significantly enlarged by reducing the time constant of the first-order inertia link and the delay link.

Based on the above analysis, we can conclude that string stability optimization of existing ACC systems should prioritize lower level controllers rather than upper level controllers.

CRediT authorship contribution statement

Tiancheng Ruan: Conceptualization of this study, Methodology, Writing - Original draft preparation, Resources, Software. **Hao Wang:** Formal analysis, Funding acquisition, Supervision, Writing - review & editing. **Linjie Zhou:** Data curation, Investigation. **Rui Jiang:** Data curation, Writing - review & editing. **Xinjian Xie:** Formal analysis, Writing - Original draft preparation.

Acknowledgment

This research was sponsored by the National Key Research and Development Program of China (No. 2019YFB1600200), National Science Foundation of China (No. 51878161, No. 71931002 and No.52072067).

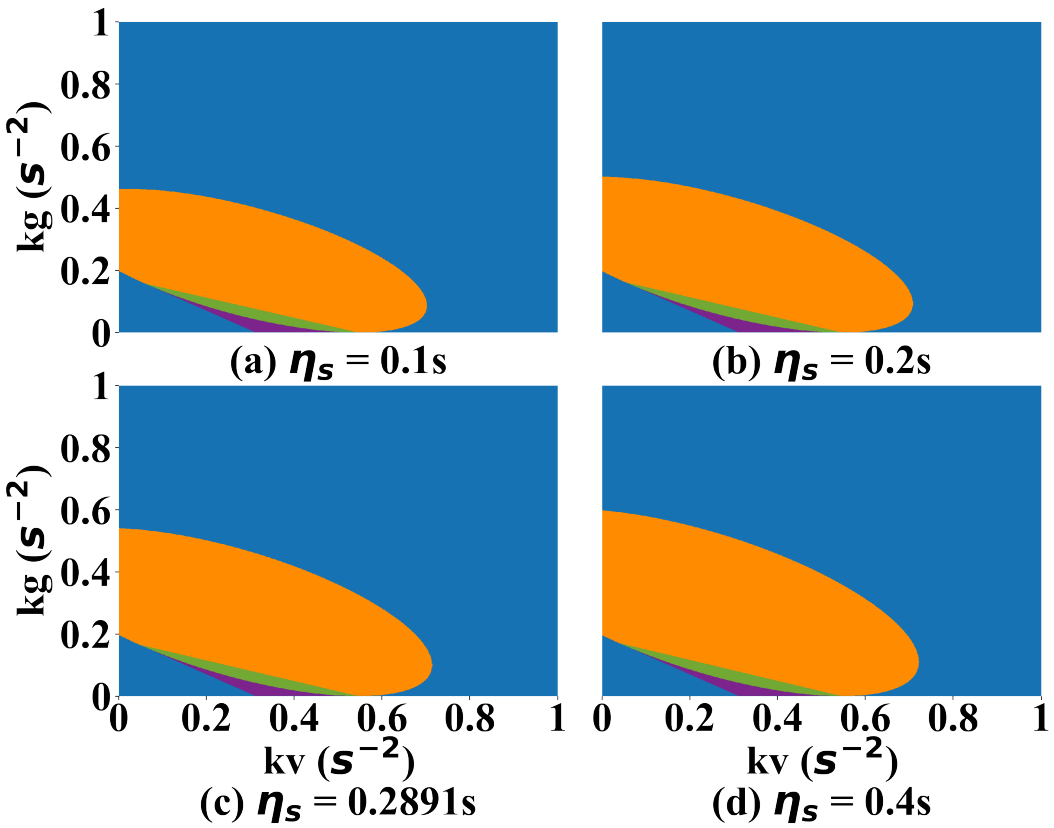


Figure 10: Stability diagram in the space $(k_g - k_v)$ under different η_s , where purple region depicts the stability region under stability type I; orange region depicts stability type II; green region depicts both satisfied type I and II; blue region depicts instability.

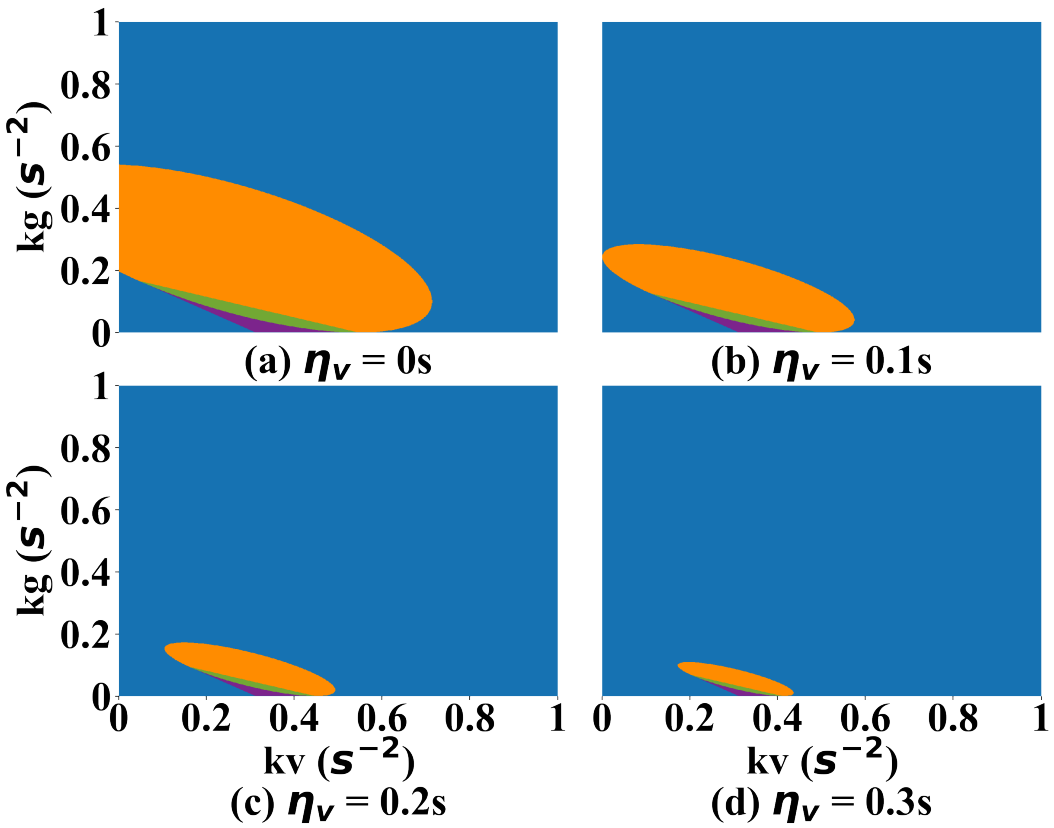


Figure 11: Stability diagram in the space $(k_g - k_v)$ under different η_v , where purple region depicts the stability region under stability type I; orange region depicts stability type II; green region depicts both satisfied type I and II; blue region depicts instability.

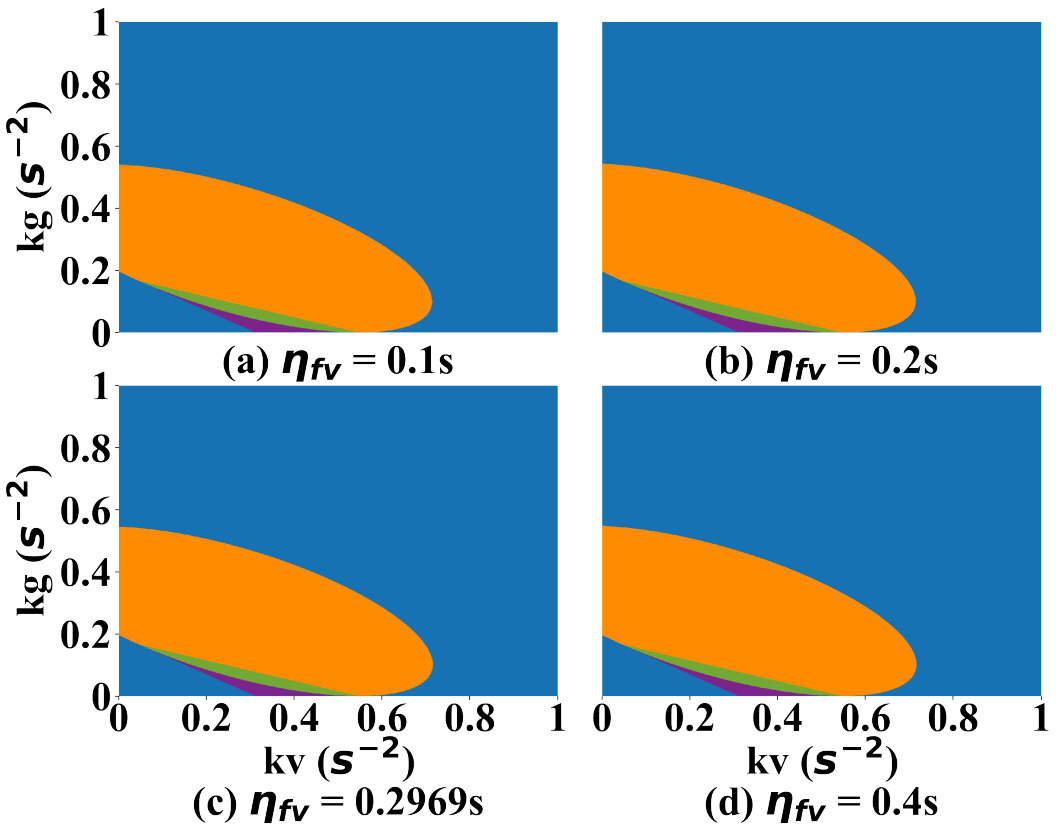


Figure 12: Stability diagram in the space $(k_g - k_v)$ under different η_{fv} , where purple region depicts the stability region under stability type I; orange region depicts stability type II; green region depicts both satisfied type I and II; blue region depicts instability.

References

- van Arem, B., Abbas, M.M., Li, X., Head, L., Zhou, X., Chen, D., Bertini, R., Mattingly, S.P., Wang, H., Orosz, G., 2016. Integrated traffic flow models and analysis for automated vehicles, in: *Road Vehicle Automation 3*. Springer, pp. 249–258.
- Bansal, P., Kockelman, K.M., 2017. Forecasting Americans' long-term adoption of connected and autonomous vehicle technologies. *Transportation Research Part A: Policy and Practice* 95, 49–63.
- Bian, Y., Zheng, Y., Ren, W., Li, S.E., Wang, J., Li, K., 2019. Reducing time headway for platooning of connected vehicles via V2V communication. *Transportation Research Part C: Emerging Technologies* 102, 87–105.
- Choi, S.B., Devlin, P., 1995. Throttle and brake combined control for intelligent vehicle highway systems. Technical Report.
- Choi, S.B., Hedrick, J.K., 1995. Vehicle longitudinal control using an adaptive observer for automated highway systems, in: *Proceedings of 1995 American Control Conference-ACC'95*, IEEE. pp. 3106–3110.
- Ciuffo, B., Mattas, K., Makridis, M., Albano, G., Anesiadou, A., He, Y., Josvai, S., Komnos, D., Pataki, M., Vass, S., Szalay, Z., 2021. Requiem on the positive effects of commercial adaptive cruise control on motorway traffic and recommendations for future automated driving systems. *Transportation Research Part C: Emerging Technologies* 130, 103305. URL: <https://www.sciencedirect.com/science/article/pii/S0968090X21003144>, doi:<https://doi.org/10.1016/j.trc.2021.103305>.
- Darbha, S., 2003. On the synthesis of controllers for continuous time LTI systems that achieve a non-negative impulse response. *Automatica* 39, 159–165.
- Darbha, S., Rajagopal, K.R., 1999. Intelligent cruise control systems and traffic flow stability. *Transportation Research Part C: Emerging Technologies* 7, 329–352.
- Dey, K.C., Yan, L., Wang, X., Wang, Y., Shen, H., Chowdhury, M., Yu, L., Qiu, C., Soundararaj, V., 2015. A review of communication, driver characteristics, and controls aspects of cooperative adaptive cruise control (CACC). *IEEE Transactions on Intelligent Transportation Systems* 17, 491–509.
- Feng, S., Zhang, Y., Li, S.E., Cao, Z., Liu, H.X., Li, L., 2019. String stability for vehicular platoon control: Definitions and analysis methods. *Annual Reviews in Control* 47, 81–97.
- Flores, C., Milanés, V., 2018. Fractional-order-based ACC/CACC algorithm for improving string stability. *Transportation Research Part C: Emerging Technologies* 95, 381–393. URL: <https://www.sciencedirect.com/science/article/pii/S0968090X18307150>, doi:<https://doi.org/10.1016/j.trc.2018.07.026>.
- Gunter, G., Janssen, C., Barbour, W., Stern, R.E., Work, D.B., 2019. Model-based string stability of adaptive cruise control systems using field data. *IEEE Transactions on Intelligent Vehicles* 5, 90–99.
- Hedrick, J.K., McMahan, D.H., Swaroop, D., 1993. Vehicle modeling and control for automated highway systems .
- Hedrick, J.K., McMahon, D., Narendran, V., Swaroop, D., 1991. Longitudinal vehicle controller design for IVHS systems, in: *1991 American Control Conference*, IEEE. pp. 3107–3112.
- Jin, I.G., Orosz, G., 2014. Dynamics of connected vehicle systems with delayed acceleration feedback. *Transportation Research Part C: Emerging Technologies* 46, 46–64.
- Jin, I.G., Orosz, G., 2016. Optimal control of connected vehicle systems with communication delay and driver reaction time. *IEEE Transactions on Intelligent Transportation Systems* 18, 2056–2070.
- Kollár, I., Pintelon, R., Schoukens, J., 2006. Frequency domain system identification toolbox for MATLAB: Characterizing nonlinear errors of linear models. *IFAC Proceedings Volumes* 39, 726–731.
- Lee, D., Lee, S., Chen, Z., Park, B.B., Shim, D.H., 2021. Design and field evaluation of cooperative adaptive cruise control with unconnected vehicle in the loop. *Transportation Research Part C: Emerging Technologies* 132, 103364. URL: <https://www.sciencedirect.com/science/article/pii/S0968090X21003661>, doi:<https://doi.org/10.1016/j.trc.2021.103364>.
- Li, T., Chen, D., Zhou, H., Xie, Y., Laval, J., 2022. Fundamental diagrams of commercial adaptive cruise control: Worldwide experimental evidence. *Transportation Research Part C: Emerging Technologies* 134, 103458. doi:[10.1016/J.TRC.2021.103458](https://doi.org/10.1016/J.TRC.2021.103458).
- Ljung, L., 1995. System identification toolbox: User's guide. Citeseer.
- Loke, S.W., 2019. Cooperative Automated Vehicles: A Review of Opportunities and Challenges in Socially Intelligent Vehicles beyond Networking. *IEEE Transactions on Intelligent Vehicles* 4, 509–518. doi:[10.1109/TIV.2019.2938107](https://doi.org/10.1109/TIV.2019.2938107), arXiv:1710.00461.
- Milanés, V., Shladover, S.E., 2014. Modeling cooperative and autonomous adaptive cruise control dynamic responses using experimental data. *Transportation Research Part C: Emerging Technologies* 48, 285–300.
- Montanino, M., Monteil, J., Punzo, V., 2021. From homogeneous to heterogeneous traffic flows: Lp String stability under uncertain model parameters. *Transportation Research Part B: Methodological* 146, 136–154. URL: <https://doi.org/10.1016/j.trb.2021.01.009>, doi:[10.1016/j.trb.2021.01.009](https://doi.org/10.1016/j.trb.2021.01.009).
- Montanino, M., Punzo, V., 2021. On string stability of a mixed and heterogeneous traffic flow: A unifying modelling framework. *Transportation Research Part B: Methodological* 144, 133–154.
- Naus, G.J.L., Vugts, R.P.A., Ploeg, J., van De Molengraft, M.J.G., Steinbuch, M., 2010. String-stable CACC design and experimental validation: A frequency-domain approach. *IEEE Transactions on vehicular technology* 59, 4268–4279.
- Navas, F., Milanés, V., 2019. Mixing V2V- and non-V2V-equipped vehicles in car following. *Transportation Research Part C: Emerging Technologies* 108, 167–181. URL: <https://doi.org/10.1016/j.trc.2019.08.021>, doi:[10.1016/j.trc.2019.08.021](https://doi.org/10.1016/j.trc.2019.08.021).
- Ngoduy, D., 2013a. Analytical studies on the instabilities of heterogeneous intelligent traffic flow. *Communications in Nonlinear Science and Numerical Simulation* 18, 2699–2706.
- Ngoduy, D., 2013b. Instability of cooperative adaptive cruise control traffic flow: A macroscopic approach. *Communications in Nonlinear Science and Numerical Simulation* 18, 2838–2851. URL: <http://dx.doi.org/10.1016/j.cnsns.2013.02.007>, doi:[10.1016/j.cnsns.2013.02.007](http://dx.doi.org/10.1016/j.cnsns.2013.02.007).
- Ozdemir, A.A., Gumussoy, S., 2017. Transfer function estimation in system identification toolbox via vector fitting. *IFAC-PapersOnLine* 50, 6232–6237.

- Paparrizos, J., Gravano, L., 2015. k-shape: Efficient and accurate clustering of time series, in: Proceedings of the 2015 ACM SIGMOD international conference on management of data, pp. 1855–1870.
- Ploeg, J., Scheepers, B.T.M., Van Nunen, E., Van de Wouw, N., Nijmeijer, H., 2011. Design and experimental evaluation of cooperative adaptive cruise control, in: 2011 14th International IEEE Conference on Intelligent Transportation Systems (ITSC), IEEE. pp. 260–265.
- Qin, Y., Wang, H., 2021. Analytical framework of string stability of connected and autonomous platoons with electronic throttle angle feedback. *Transportmetrica A: Transport Science* 17, 59–80.
- Qin, Y., Wang, H., Ran, B., 2018. Stability Analysis of Connected and Automated Vehicles to Reduce Fuel Consumption and Emissions. *Journal of Transportation Engineering, Part A: Systems* 144, 04018068. doi:10.1061/j.tectbs.0000196.
- Rajamani, R., 2011. Vehicle dynamics and control. Springer Science & Business Media.
- Ruan, T., Zhou, L., Wang, H., 2021. Stability of heterogeneous traffic considering impacts of platoon management with multiple time delays. *Physica A: Statistical Mechanics and its Applications* 583, 126294.
- Sarker, A., Shen, H., Rahman, M., Chowdhury, M., Dey, K., Li, F., Wang, Y., Narman, H.S., 2019. A review of sensing and communication, human factors, and controller aspects for information-aware connected and automated vehicles. *IEEE transactions on intelligent transportation systems* 21, 7–29.
- Schölkopf, B., Platt, J.C., Shawe-Taylor, J., Smola, A.J., Williamson, R.C., 2001. Estimating the support of a high-dimensional distribution. *Neural computation* 13, 1443–1471.
- Schölkopf, B., Smola, A.J., Bach, F., 2002. Learning with kernels: support vector machines, regularization, optimization, and beyond. MIT press.
- Schölkopf, B., Williamson, R.C., Smola, A., Shawe-Taylor, J., Platt, J., 1999. Support vector method for novelty detection. *Advances in neural information processing systems* 12.
- Schrink, D., Eisele, B., Lomax, T., 2012. TTI's 2012 urban mobility report. Texas A&M Transportation Institute. The Texas A&M University System 4.
- Shang, M., Rosenblad, B., Stern, R., 2022. A Novel Asymmetric Car Following Model for Driver-Assist Enabled Vehicle Dynamics. *IEEE Transactions on Intelligent Transportation Systems*.
- Shang, M., Stern, R.E., 2021. Impacts of commercially available adaptive cruise control vehicles on highway stability and throughput. *Transportation Research Part C: Emerging Technologies* 122, 102897. doi:10.1016/J.TRC.2020.102897.
- Swaroop, D., 1994. String stability of interconnected systems: An application to platooning in automated highway systems.
- Treiber, M., Kesting, A., 2011. Evidence of convective instability in congested traffic flow: A systematic empirical and theoretical investigation. *Procedia-Social and Behavioral Sciences* 17, 683–701.
- Wang, C., Gong, S., Zhou, A., Li, T., Peeta, S., 2018. Cooperative adaptive cruise control for connected autonomous vehicles by factoring communication-related constraints. *Transportation Research Procedia* 38, 242–262. URL: <https://doi.org/10.1016/j.trpro.2019.05.014>, arXiv:1807.07232.
- Wang, M., 2018. Infrastructure assisted adaptive driving to stabilise heterogeneous vehicle strings. *Transportation Research Part C: Emerging Technologies* 91, 276–295. URL: <https://doi.org/10.1016/j.trc.2018.04.010>, doi:10.1016/j.trc.2018.04.010.
- Wang, Z., Bian, Y., Shladover, S.E., Wu, G., Li, S.E., Barth, M.J., 2019. A survey on cooperative longitudinal motion control of multiple connected and automated vehicles. *IEEE Intelligent Transportation Systems Magazine* 12, 4–24.
- Wilson, R.E., 2008. Mechanisms for spatio-temporal pattern formation in highway traffic models. *Philosophical Transactions of the Royal Society A: Mathematical, Physical and Engineering Sciences* 366, 2017–2032.
- Wilson, R.E., Ward, J.A., 2011. Car-following models: fifty years of linear stability analysis—a mathematical perspective. *Transportation Planning and Technology* 34, 3–18.
- Xiao, L., Gao, F., 2011. Practical string stability of platoon of adaptive cruise control vehicles. *IEEE Transactions on Intelligent Transportation Systems* 12, 1184–1194. doi:10.1109/TITS.2011.2143407.
- Yao, Z., Xu, T., Jiang, Y., Hu, R., 2021. Linear stability analysis of heterogeneous traffic flow considering degradations of connected automated vehicles and reaction time. *Physica A: Statistical Mechanics and its Applications* 561, 125218.
- Ye, L., Yamamoto, T., 2018. Impact of dedicated lanes for connected and autonomous vehicle on traffic flow throughput. *Physica A: Statistical Mechanics and its Applications* 512, 588–597.
- Yu, H., Jiang, R., He, Z., Zheng, Z., Li, L., Liu, R., Chen, X., 2021. Automated vehicle-involved traffic flow studies: A survey of assumptions, models, speculations, and perspectives. *Transportation Research Part C: Emerging Technologies* 127, 103101. doi:10.1016/j.trc.2021.103101.
- Zheng, Y., Li, S.E., Wang, J., Cao, D., Li, K., 2015. Stability and scalability of homogeneous vehicular platoon: Study on the influence of information flow topologies. *IEEE Transactions on intelligent transportation systems* 17, 14–26.
- Zhong, Z., Lee, E.E., Nejad, M., Lee, J., 2020. Influence of CAV clustering strategies on mixed traffic flow characteristics: An analysis of vehicle trajectory data. *Transportation Research Part C: Emerging Technologies* 115, 102611.
- Zhou, L., Ruan, T., Ma, K., Dong, C., Wang, H., 2021. Impact of CAV platoon management on traffic flow considering degradation of control mode. *Physica A: Statistical Mechanics and its Applications* 581. doi:10.1016/j.physa.2021.126193.
- Zhou, Y., Ahn, S., 2019. Robust local and string stability for a decentralized car following control strategy for connected automated vehicles. *Transportation Research Part B: Methodological* 125, 175–196. URL: <https://doi.org/10.1016/j.trb.2019.05.003>, doi:10.1016/j.trb.2019.05.003.
- Zhou, Y., Ahn, S., Chitturi, M., Noyce, D.A., 2017. Rolling horizon stochastic optimal control strategy for ACC and CACC under uncertainty. *Transportation Research Part C: Emerging Technologies* 83, 61–76. URL: <https://www.sciencedirect.com/science/article/pii/S0968090X17301997>, doi:<https://doi.org/10.1016/j.trc.2017.07.011>.